JOURNAL OF GEOPHYSICAL RESEARCH, VOL. 92, NO. C7, PAGES 6825–6835, JUNE 30, 1987

Evolution of Microwave Sea Ice Signatures During Early Summer and Midsummer in the Marginal Ice Zone

R. G. ONSTOTT,[1] T. C. GRENFELL,[2] C. MATZLER,[3] C. A. LUTHER,[4] AND E. A. SVENDSEN[5]

Emissivities at frequencies from 5 to 94 GHz and backscatter at frequencies from 1 to 17 GHz were measured from sea ice in Fram Strait during the Marginal Ice Zone Experiment in June and July of 1983 and 1984. The ice observed was primarily multiyear; the remainder, first-year ice, was often deformed. Results from this active and passive microwave study include the description of the evolution of the sea ice during early summer and midsummer; the absorption properties of summer snow; the interrelationship between ice thickness and the state and thickness of snow; and the modulation of the microwave signature, especially at the highest frequencies, by the freezing of the upper few centimeters of the ice.

INTRODUCTION

Active and passive microwave remote sensing of sea ice offer the potential of obtaining synoptic data of large expanses of remote, ice-covered oceans under all weather conditions irrespective of the amount of solar illumination. This is of particular importance for Arctic applications where much of the polar ice canopy is under clouds or in darkness.

Numerous late winter and spring experiments have concentrated on the ability to classify ice types, to detect scientifically interesting features, and to describe ice field kinematics and dynamics. Efforts also focused on a determination of optimum frequencies, polarizations, and incidence angles and on the development of algorithms for extracting geophysical parameters from sea ice imagery. *Campbell et al.* [1975], *Ramseier and Lapp* [1980], and *Livingstone et al.* [1981] conclude their studies by stating that many features, including ice types, ridges and roughness features, lead and polynya formations, and icebergs, have distinct signatures which are observed using active and passive microwave sensors. They also present the hypothesis that a combination of multifrequency, active and passive (microwave and millimeter wave) sensors is especially valuable for extracting information about the state of the ice. They present the hypothesis that emissivity and backscatter are influenced by different aspects of the sea ice structure and that the relationship between microwave frequency and penetration depth may be exploited robustly.

The more limited experimentation by *Gray et al.* [1982], *Onstott et al.* [1982], *Onstott and Gogineni* [1985], *Grenfell and Lohanick* [1985], and *Lohanick and Grenfell* [1986] during the summer melt period illustrate the extreme difficulty in detecting and classifying sea ice features when surface conditions change rapidly. They concluded that use of microwave sensors to classify sea ice type and features unambiguously requires understanding of the emissivity and reflectivity characteristics of the various ice types and that to understand the electromagnetic characteristics requires the understanding of sea ice physical properties.

Intensive measurement of summer sea ice signatures were made in Fram Strait during June and July of 1983 and 1984. These data were acquired during participation in the Marginal Ice Zone Experiment (MIZEX) [*Johannessen and Horn*, 1984], a multinational interdisciplinary effort to study the air-sea-ice interaction processes in the transition region where the pack ice meets the open ocean. An objective of MIZEX is to define the geophysical processes which govern these interactions and to understand how these interactions influence ice edge location, ice morphology, ice sheet deformation, and ice band formation.

This paper presents a comprehensive discussion of the summer microwave signatures of the major classes of Arctic sea ice in the marginal ice zone (MIZ) and their relationship to snow and ice physical properties. The discussion begins by examining winter and spring signatures using data from previous experiments. Electromagnetic interaction arguments are developed to describe the effect of summer metamorphosis on sea ice signatures. The discussions provided may also be extended to include sea ice scenes found in other regions.

ELECTRICAL PROPERTIES OF SEA ICE AND SNOW

Frozen sea water, sea ice, is a lossy dielectric. It consists of pure ice, liquid brine, and air. Snow blankets the top of this low-density solid. During winter, the microwave signatures of the desalinated multiyear ice are clearly different from those of the saline first-year ice. The situation in summer is more complex; this is the time of desalination, of melting snow and ice, of melt pool formation, and of the melt-and-freeze cycling of the upper surface. Microwave signatures track these meteorologically induced melt-and-freeze cycles.

Important in remote sensing science is how the electrical and physical properties of snow and ice are modified as they experience summer melt. The physial parameters which influence the microwave observables are snow wetness, snow grain size, snow density, and snow and ice roughness. Sensor parameters, such as wavelength, polarization, and incidence angle, also influence the intensity of backscatter and emission. In the microwave and millimeter wave region the electrical properties of dry snow (a mixture of ice crystals and air) are approximately frequency independent. Following *Matzler* [1985], who summarizes the results of many investigations,

[1] Radar Science Laboratory, Advanced Concepts Division, Environmental Research Institute of Michigan, Ann Arbor, Michigan.
[2] Department of Atmospheric Sciences, University of Washington, Seattle.
[3] Institute of Applied Physics, University of Bern, Bern, Switzerland.
[4] Office of Naval Research, Arctic Sciences, Washington, D. C.
[5] Geophysical Institute and Nansen Ocean and Remote Sensing Center, University of Bergen, Solheimsvik, Norway.

Paper number 7C0197.
0148-0227/87/007C-0197$05.00

TABLE 1. Brief Summary of Ice Descriptions During MIZEX 1983 and 1984

Ice Type*	Ice Thickness Range, cm	Snow Thickness Range, cm	Snow Thickness Average, cm	Ice Salinity in Top 10 cm, ‰	Ice Salinity in Top 40 cm, ‰
MY	174–536	3–65	29	0–1	0–1
TFY	175–236	2–20	10	1–4	4–5
MFY	90–120	2–14	6	1	2–3
ThFY	38–70	2–6	4	3–4	4–5

*See text for explanation of abbreviations.

the real part of the dielectric constant expressed as a function of snow density is

$$\varepsilon_{\text{dry}}' = 1 + \frac{1.6\rho}{(1 - 0.35\rho)} \tag{1}$$

In (1), ρ is the density of dry snow in kilograms per cubic meter. Three important notes are as follows: (1) freshly deposited snow quickly attains a density of at least 330 kg m^{-3}, (2) during MIZEX, densities in the dry surface layer were about 400–500 kg m^{-3} for old snow and less than 100 kg m^{-3} for new snow, and (3) the density of pure solid ice is 916 kg m^{-3}.

The imaginary part of the complex dielectric constant is important in that it is one of the parameters which describe the absorption properties of a dielectric medium. The complex dielectric constant of wet snow is strongly dependent on frequency, density, and wetness [*Matzler*, 1985]. It may be expressed using the simple Debye relaxation spectra by neglecting the low dielectric losses of dry snow as

$$\varepsilon = \varepsilon_{\text{dry}}' + \frac{0.23w}{1 + if/f_0} \tag{2}$$

where w is the percent volumetric liquid water content, f_0 is 10 GHz (relaxation frequency of wet snow), and f is frequency in gigahertz.

The propagation distance through a medium over which the intensity is reduced by e^{-1} is often referred to as the penetration depth (PD). The penetration depth is given by

$$\text{PD} = 0.5\alpha^{-1} \tag{3}$$

where

$$\alpha = \frac{2\pi}{\lambda} |\text{Im}\ [\sqrt{e}]| \tag{4}$$

In (4), λ is the free space wavelength. Ignoring scattering losses, a 9-dB round-trip loss is experienced in propagating over this distance. It is also important to note that up to two or three penetration depths may need to be considered when examining potential contributions to the microwave signature.

Ice Conditions and Experiment Description

The Fram Strait is the key outflow region of the Arctic Basin. Ice may originate from any region of the basin. This is not a typical MIZ and is unique both oceanographically and in its sea ice characteristics. Hence both ice physical and microwave properties may be quite diverse, since the area of origin strongly influences the environment in which an ice sheet grows.

As ice from the very close pack approaches the margins, it breaks up into smaller floes. Still nearer the ice edge, higher-frequency components of swell are greater in amplitude, and floes are further reduced in size, often into patches of small, similarly sized floes. During MIZEX, sea ice was investigated throughout the region from the edge of the central pack to the extreme ice margin. It is worth noting that our observations show that ice and snow conditions at sites close to the edge of the pack and ice in the interior of the MIZ are similar.

Most of the ice in the MIZ has experienced dynamic forcing, which increases surface and subsurface topography as well as floe thickness prior to entering Fram Strait. Deformed ice is found in the form of pressure ridges and rubble, each of which has its own roughness scale. Ice may also have regions of surface and subsurface meltwater pools and areas of flat ice and mounds. The microwave properties of these diverse scenes may be equally varied.

The major summer sea ice forms found during June and July included (1) multiyear (MY) ice which has survived at least one summer's melt and typically has a thickness greater than 2.5, (2) thick first-year (TFY) ice which began growing early in the season and attains a thickness greater than 120 cm, (3) medium first-year (MFY) ice which began growing later in the growing season, reaching a thickness of 70–120 cm, and (4) thin first-year (ThFY) ice which began growing late in the season and has a thickness of 30–70 cm.

Floe size ranged from small, a horizontal extent of 20–100 m, to giant, a horizontal extent greater than 10 km. Most of the ice was multiyear. The proportion of first-year (FY) ice was difficult to estimate but was probably less than one third of the total ice cover. Because of the melting conditions, new ice formation in leads was not significant and would not affect lead signatures. Snowpack was typically heavy and wet, with depths up to 65 cm on many MY ice floes. This is very thick by Arctic standards. A more detailed description of the range of conditions found during MIZEX is assembled in Table 1. During the experiment period the snowpack and ice sheets underwent a transition from late spring to summer melt conditions. Air temperatures were typically within 2° of 0°C. Extremes ranged from −10°C to +4°C. Measured using alcohol calorimetry, volumetric snow wetness in both the interior and the upper few centimeters ranged from 0% to 10%, except for variations in a thin surface layer. The bulk snow wetness stayed at about 5–6% over much of the experiment duration. Figure 1 shows the microwave penetration depths for the con-

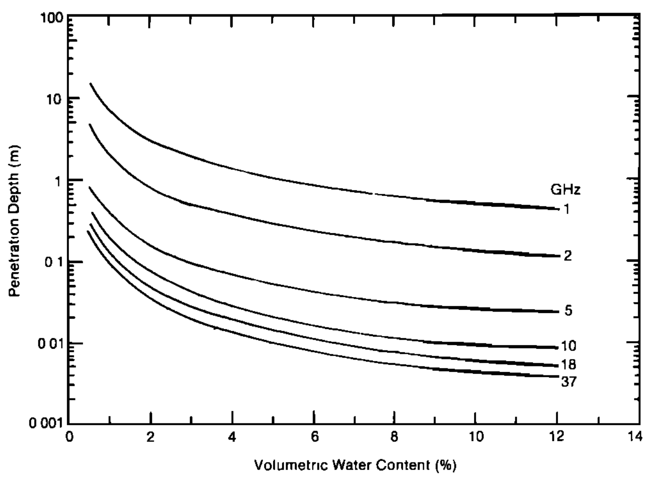

Fig. 1. Penetration depth for snow with a density of 385 kg m^{-3} for frequencies between 1 and 37 GHz. Calculations are based on experimental data acquired and results published by *Matzler* [1985], *Hallikanen et al.* [1984] and *Tiuri et al.* [1984].

TABLE 2. In Situ Microwave Sensor Description and Specification

	University of Washington	University of Kansas	University of Bern
Sensor	radiometer*	scatterometer†	radiometer‡
Sensor type	Dicke and total power	FM-CW	Dicke
Icebreaker/year	PB and PS in 1983, PQ in 1984	PB and PS in 1983, PS in 1984	PS in 1983
Platform	sled	helicopter and ship	ship
Frequencies, GHz	6, 10, 18, 37, and 90	1.5, 5.2, 9.6, 13.6, and 16.6	4.9, 19.4, 21, 35, and 94
Polarization	V and H	VV, HH, and HV	V and H
Nadir viewing angle	20°–60°	0°–75°	20°–60°
Precision	1–5 K	1 dB	0.1–1.2 K
Accuracy	3–7 K	2 dB	1 K
Beamwidth	15°	2°–11°	9°–10°
Height	$1\frac{1}{2}$ m	15–45 m	17 m
Calibration	sky and internal	Luneberg lens reflector	sky and internal

PB, Polarbjorn; PS, Polarstern; PQ, Polarqueen.
*Radiometer named UW/RAD.
†Scatterometer named HELOSCAT.
‡Radiometer named PAMIR.

ditions described here, shown as a function of snow wetness and frequency. Flooding of the ice-snow interface with fresh water was occurring due to continual snowpack ablation during much of the investigation.

Our observations show that snow cover thickness of ThFY (2–6 cm), MFY (6–15 cm), TFY (6–20 cm), and MY (15–65 cm) ice was variable. New snow also fell during these investigations (0.5–1 cm). Snow on pressure ridges and other elevated features was shallow and consisted of very coarse grains up to 2 cm in size. We feel that grains of this size must have formed under the temperature gradient metamorphism during the previous winter. A hexagonal shape indicated a slight rounding by melt metamorphism. Old snow was similar to firn, with grain diameters of 1 mm. Snow crystal sizes of 0.5–2 mm diameter were typical. First-year ice and advanced areas of melt on MY ice showed 3–5 mm diameter with occasional ice crystal globes exceeding a diameter of 1 cm.

Salinities in the upper layer of the ice sheet were much less than 1‰ for MY and around 2‰ in the case of FY ice, typically. In 1984 the FY upper ice sheet salinity decreased over the experiment duration, and the MY ice salinity increased to about 0.3‰ [*Tucker et al.*, this issue].

Measurement Approach

The integration of microwave measurements by a comprehensive set of satellite, aircraft, ship, and surface-based sensors with sea ice scene characterization measurements is a fundamental accomplishment of the MIZEX Remote Sensing Program [*MIZEX Group*, 1986]. All sensor parameters overlap well by design. Imagery was collected of specifically chosen representative ice floes on which coincident in situ surface, shipboard, and helicopter-borne measurements of scattering and emission characteristics and ice physical properties were made. For detailed discussion of the near-surface sensor parameters and experimental procedure, refer to *Grenfell and Lohanick* [1985], *Matzler et al.* [1984], *Gogineni et al.* [1984], and Table 2.

The surface-based measurements include (1) snow thickness, wetness, density, physical construction, dielectric constant, and temperature, (2) ice thickness, wetness, density, physical construction, salinity profile, temperature profile, surface roughness, state of deformation, and dielectric constant, (3) general floe topography, and (4) the spatial distribution of meltwater on the ice sheet.

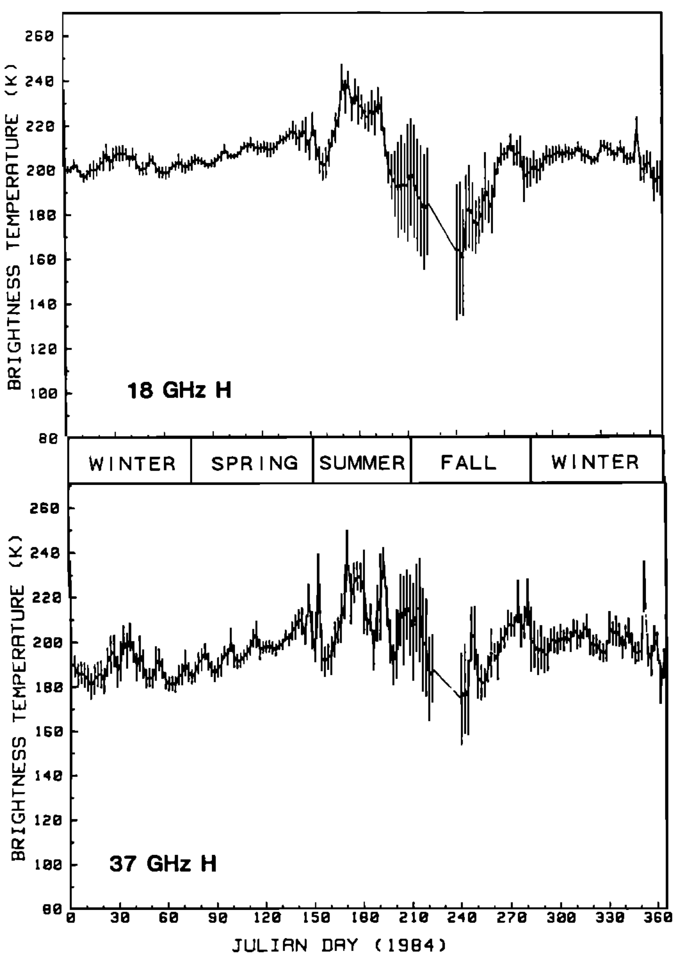

Fig. 2. Time series of average Nimbus 7 H polarization brightness temperatures at 18 GHz and 37 GHz for a 300 km by 300 km region in the Greenland Sea near the MIZEX study area during 1984. The short vertical lines represent one standard deviation (D. J. Cavalieri, NASA, Goddard, unpublished data, 1986).

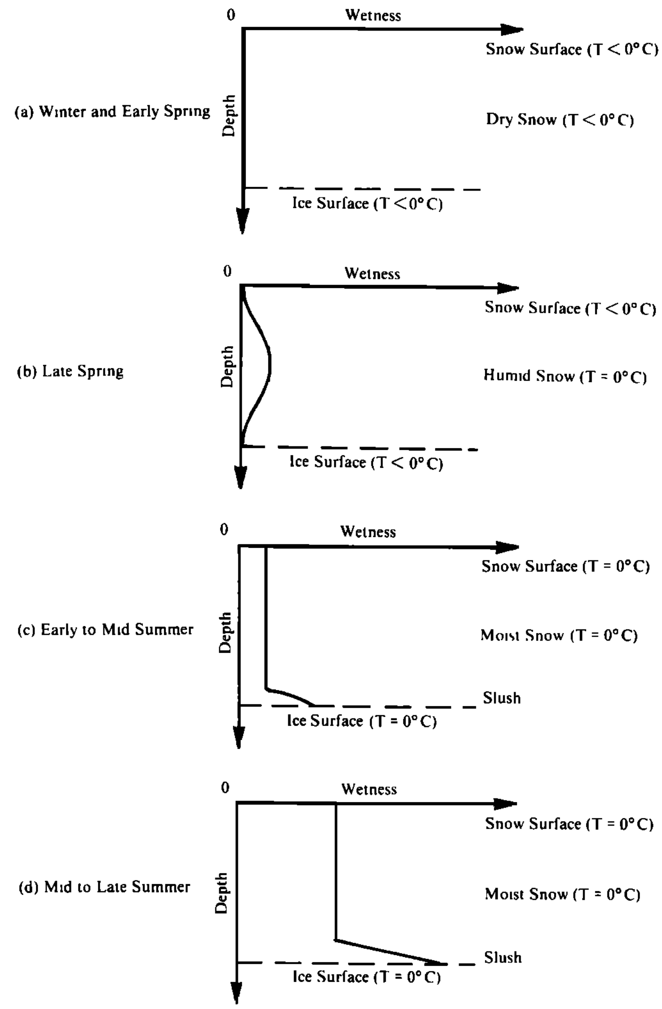

Fig. 3. Free water fraction versus depth for snow on sea ice, illustrating conditions encountered during (*a*) winter and early spring, (*b*) late spring, (*c*) early summer, and (*d*) midsummer.

Satellite-Acquired Sea Ice Temporal Signatures

The mean and standard deviation of the brightness temperatures at 18 GHz and 37 GHz with horizontal polarization of sea ice as derived from the Nimbus 7 scanning multichannel microwave radiometer (SMMR) in a 300 km by 300 km region in Fram Strait in the vicinity of the MIZ are shown for alternate days in Figure 2 (D. J. Cavalieri, NASA, unpublished data, 1986). These brightness temperature data show the big picture, the continuous time series record for the 1984 Arctic year. They illustrate the transition from winter to summer signatures and provide the forum from which the in situ "snapshots" are discussed.

During the cold winter months, between December and March (Julian days 335–90), the sea ice brightness temperature variations are small and are primarily due to changes in ice concentration or to variations in the physical temperatures of the radiative portion of the ice or both. Starting in April (Julian day 91) the steadily increasing spring warming trend translates into a similarly increasing scene brightness temperature. By May (Julian days 121–151) this trend was disturbed. As we observed during MIZEX, the emission at 36 GHz is very sensitive to the presence of free water and the recrystallization of the upper few centimeters of the snowpack. Weather records indicate that a series of atmospheric lows of warm air passed through this region during this critical period. Our hypothesis is that the upper layer of the snowpack experiences a metamorphism causing an enlargement of ice crystals. Once temperatures return to normal and the snowpack refreezes, the brightness temperature will be lower due to an additional scattering loss which arises from the increase in ice crystal size.

The sudden jump in brightness temperature from June 8 to 18 (Julian days 160 to 170) marks the onset of summer melt, when temperatures stabilize at about 0°C. It will be demonstrated that the new brightness temperature threshold during the first half of this period indicates a moist snowpack. In addition, the melt-freeze cycles which occur throughout the Arctic summer contribute to the wide range of brightness temperatures. By the second half of summer (beginning about Julian day 180), melt has advanced to a stage where a significant proportion of the snowpack has melted and open pools of meltwater are more numerous. The brightness temperature shows a decrease of at least 10 K (see 18-GHz data) and larger standard deviations. Standard deviations at 37 GHz are even larger, due in part to the larger number of footprints at 37 GHz than at 18 GHz in the 300 km by 300 km region. The dip in brightness temperature is then followed by an increase (about Julian day 195). This represents a very interesting and important event. Sea ice may experience periods of drying during which the areal extent of surface meltwater is reduced due to draining through cracks, thaw holes, and rotting ice. Such cycles of draining and melting were observed during MIZEX. At about the middle of July (Julian day 195) the brightness temperature shows a significant increase. We attribute this to the reduction in the areal extent of open water in melt pools and to wet air-snow and air-ice interfaces.

By the beginning of September (Julian day 244) the ice is well drained, the rapid cooling of the Arctic proceeds, the ice concentration is at its minimum, and the minimum brightness temperature for the year is reached. By the end of September, brightness temperatures have returned to wintertime conditions.

MICROWAVE SIGNATURE AND SCENE INTERCOMPARISONS

The microwave signature of the evolving summer sea ice as measured in situ is discussed for the periods of winter, late spring, early summer, and midsummer. Two additional influences, very heavy melt and rain and frozen surface crust, and included because of their ability to alter the seasonal microwave signature. Figures 3 and 4 illustrate the general distribution of wetness (liquid water content) in the snow on ice as observed during MIZEX. Cross-sectional representations of gross changes in the physical construction of the snowpack, the snow-ice interface, and the ice sheet are provided in Figures 5 and 6.

In what follows, emissivities are shown at frequencies from 5 to 94 GHz for a 50° nadir angle and horizontal (H) and vertical (V) polarizations. Radar backscatter cross sections are at frequencies from 1 to 17 GHz, at angles from 0° to 60°, and at HH polarization. Since backscatter effects at VV and HH polarizations were very similar for both FY and MY ice, we follow tradition and discuss HH polarization. Radar angular response data are shown to elucidate the strong dependence of backscatter on incidence angle. The rate of falloff of backscatter beyond vertical provides information about scene roughness and the effective dielectric constant.

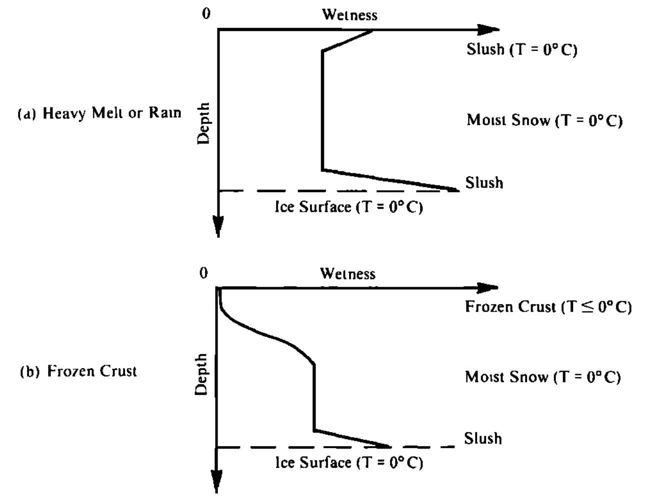

Fig. 4. Free water fraction versus depth for snow on sea ice, illustrating conditions encountered during (*a*) heavy melt or rain and (*b*) freezing of the upper snow layer.

Winter

In winter, as during most of the year, the dry snowpack and upper portion of the ice sheet are at temperatures much less than 0°C. As Figure 3*a* shows, there is no liquid water in the snow or on the ice sheet. Cross-sectional views of FY and MY ice sheets are shown in Figures 5*a* and 6*a*. Under the dry snow on undulating MY ice are flat ice, ice mounds, and depressions filled with last summer's frozen meltwater. This set of conditions serves as an excellent reference from which to examine the evolution of sea ice properties during summer.

The emissivities of FY and MY ice and calm water during winter as reported by *NORSEX Group* [1983] are shown in Figure 7*a*. Open water exhibits a large difference between emissivities at the two polarizations (Brewster angle effects) and has an emissivity which increases with increasing frequency. In contrast, the FY ice signature is close to unity and is almost independent of polarization and frequency. The multiyear ice signature is not similar to either the calm water or the FY ice. Its emissivity decreases with increasing frequency and shows a moderate separation at the different polarizations throughout the entire range of frequencies.

The radar backscatter of FY and MY ice is shown as a function of frequency at a 40° incidence angle in Figure 8*a*. These data show radar cross sections which increase linearly with increasing frequency. The radar contast between these two ice types also improves with increasing frequency. Returns from open water in the MIZ are found to be considerably lower than those from ice.

Scattering within the snow and ice reduces emission and enhances backscatter. First-year ice is very lossy because of its high salinity; hence penetration depths are small. In addition, it has few internal scatterers, such as air bubbles, whose diameters are within an order of magnitude of a wavelength. In contast, the upper portion of a MY ice sheet is composed of low-loss, almost pure ice and has significant numbers of air bubbles with diameters of 1–3 mm. The microwave signatures of sea ice at low frequencies (1–4GHz) are, for the most part, controlled by its dielectric constant and surface roughness. As wavelengths grow shorter, volume scattering from the inhomogeneities within the snow and ice becomes increasingly important. At frequencies of about 10 GHz, volume scattering begins to dominate the electromagnetic interaction process. The interested reader is referred to *Kim et al.* [1984*b*] for a detailed discussion of surface and volume scattering of sea ice.

Late Spring

By late spring, temperatures have warmed from winter lows of about −35°C; there may be periods with temperatures near

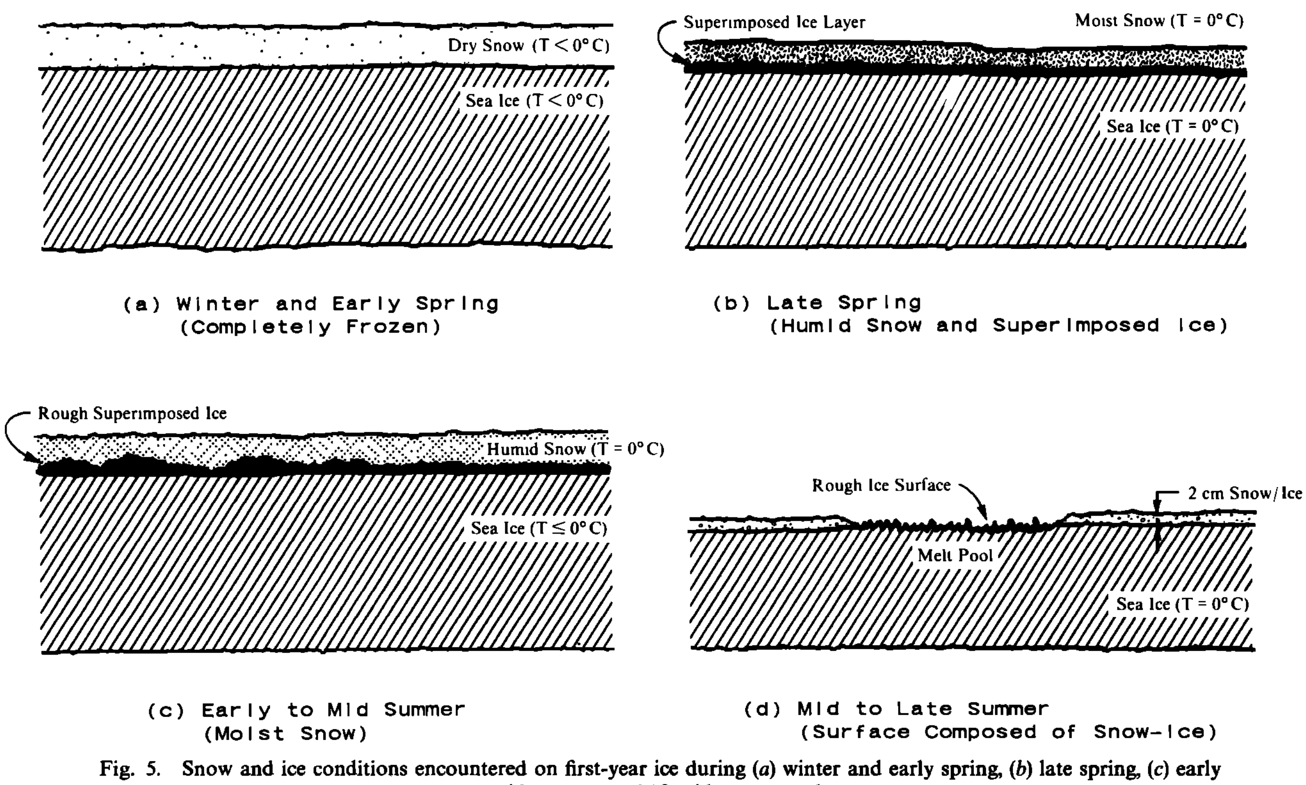

Fig. 5. Snow and ice conditions encountered on first-year ice during (*a*) winter and early spring, (*b*) late spring, (*c*) early summer to midsummer, and (*d*) midsummer to late summer.

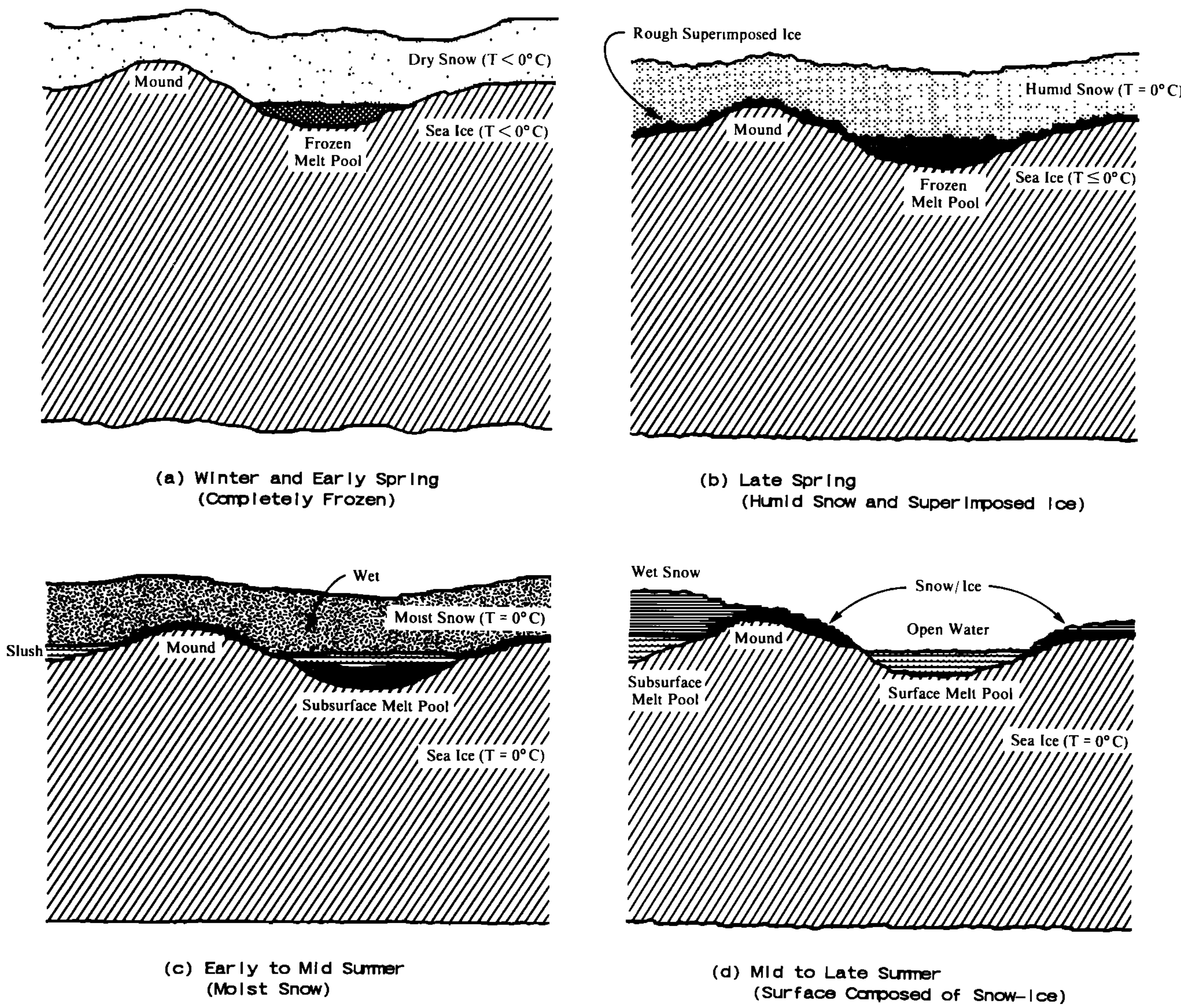

Fig. 6. Snow and ice conditions encountered on multiyear ice during (*a*) winter and early spring, (*b*) late spring, (*c*) early summer to midsummer, and (*d*) midsummer to late summer.

0°C. This rise in physical temperature is accompanied by an increase in the imaginary part of the complex dielectric constant; this increase is rapid once temperatures are within a few degrees of 0°C. During this period the interior of the snowpack becomes humid. Figure 3*b* illustrates the common occurrence of cool air above the snow, a dry snow surface layer, a humid snow interior, and a cold ice sheet surface. Moisture from the humid snow layer may collect on the cold ice surface and freeze. The superimposed ice roughens the ice-snow interface, illustrated in Figures 5*b* and 6*b*. This roughness will increase in time and influence the microwave signatures of ThFY and MFY ice during midsummer.

Signatures representative of late spring conditions are shown in Figures 7*b* and 9*a*. In contrast with winter conditions, FY and MY ice emissions are almost identical. The snow has attained a wetness sufficiently large (about 2%) that scene emissivity is determined by the snowpack and not by the cold ice sheet below.

Radar contrast at 9.6 GHz and 5.2 GHz is also reduced (see Figure 9*a*). Volume scattering, which dominated the microwave signature of MY ice during winter and early spring at 9.6 GHz, has been reduced effectively by the humid snowpack. Backscatter at 5.2 GHz is affected less because volume scattering has a reduced role at this frequency, scattering from the ice surface contributes strongly, and a penetration depth of 20 cm (3 times that at 9.6 GHz) is sufficient to continue sensing the surface and upper portion of the ice sheet.

Early Summer

Early summer may be described as the start of the 2-month period during which the mean air temperature remains close to 0°C. Summer FY and MY ice microwave signatures will be shown to be very similar. Early summer signature differences between ice types are at best subtle. The thoroughly moistened snow is at its maximum annual thickness. Free meltwater percolates through the snow and collects at the snow-ice interface, forming a thin layer of slush as shown in Figures 3*c* and 6*c* or additional superimposed ice as shown in Figure 5*c*.

During this period the emissivities of MY and FY ice share a common signature, shown in Figure 7*c*, that of an infinitely thick wet snow layer. In addition, an emissivity of almost unity was obtained at V polarization; hence the wet snow

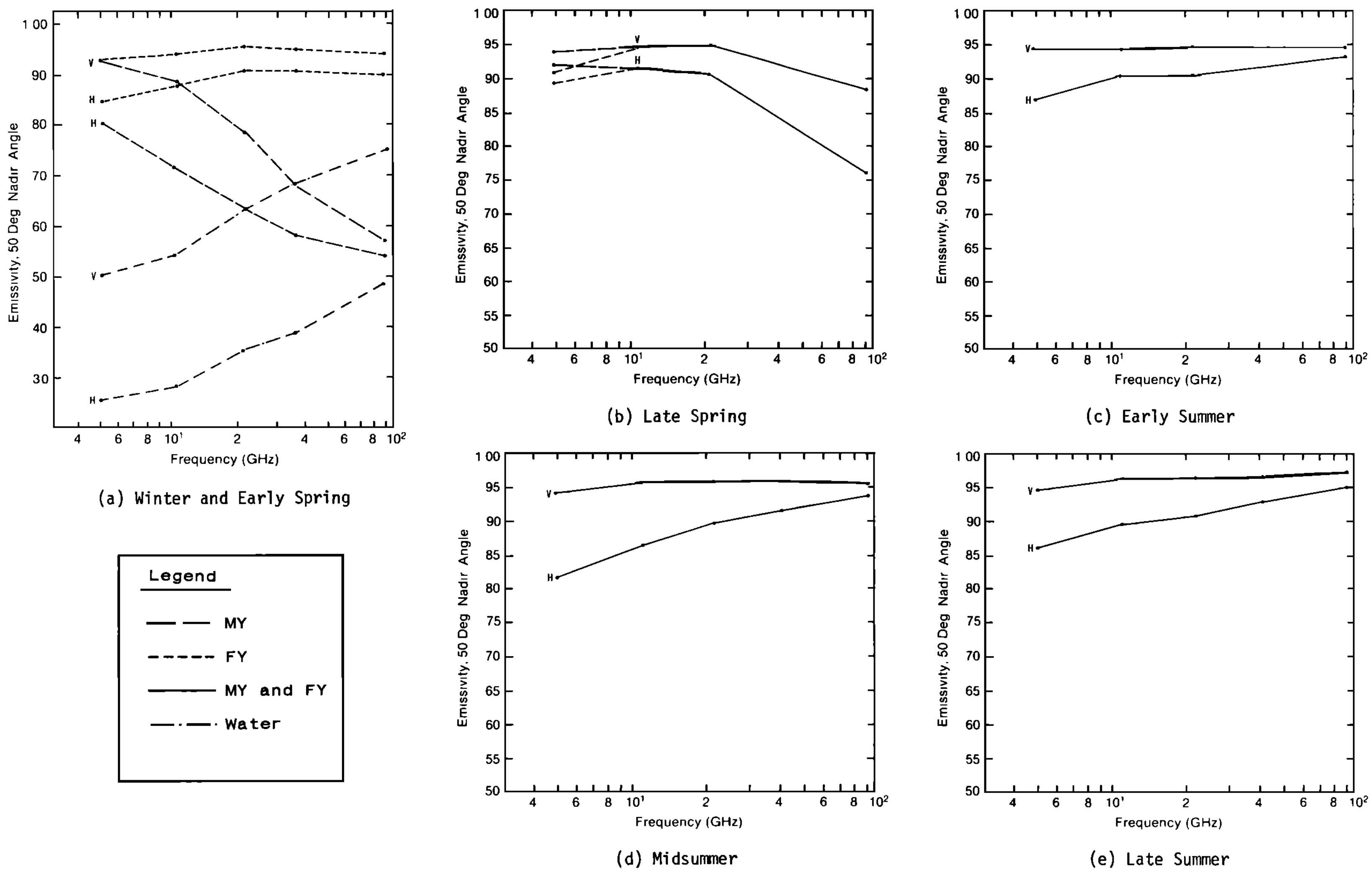

Fig. 7. Emissivity at 50° off nadir in both vertical (V) and horizontal (H) polarization versus frequency of multiyear and first-year ice (and calm water) measured during (*a*) winter with passive and active microwave and infrared radiometer (PAMIR) (*NORSEX*, 1979), (*b*) late spring with University of Washington radiometer (UW/RAD) when the surface snow is dry and the bulk wetness is 2% by volume (June 20, MIZEX '84), (*c*) early summer with UW/RAD when the associated surface free water content is about 4% by volume (June 26, MIZEX '84), (*d*) midsummer with PAMIR when the associated free water content is about 5% by volume (July 7–9, MIZEX '83) and (*e*) late summer with PAMIR when the associated free water content is about 5% by volume (July 11, MIZEX '83).

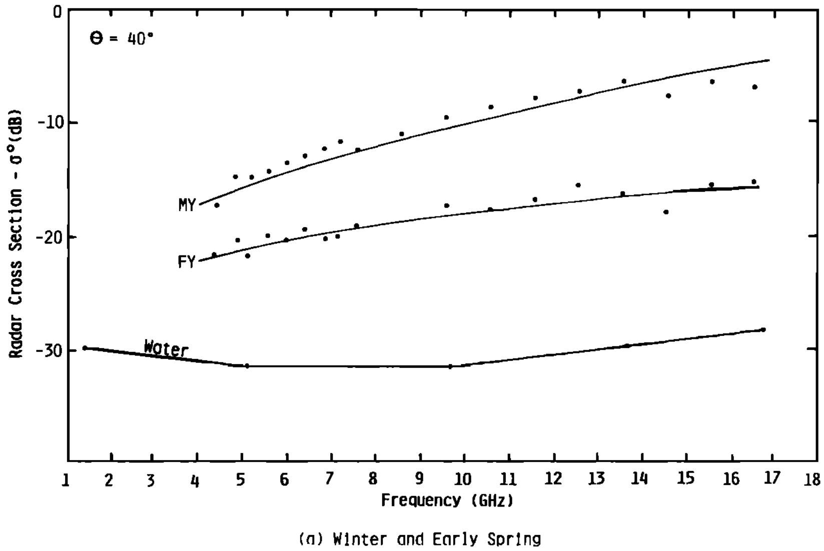

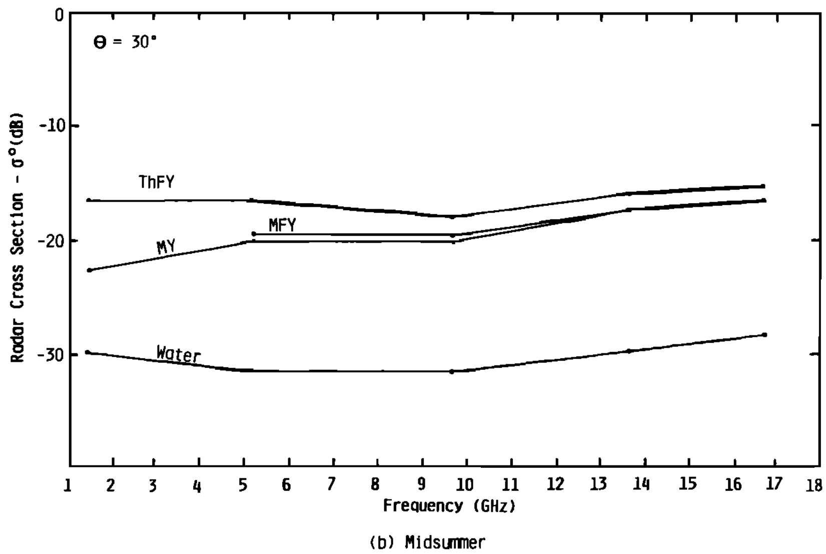

Fig. 8. Radar scattering cross section frequency response of (*a*) water and first-year (FY) and multiyear (MY) sea ice at frequencies from 4 to 17 GHz at HH polarization acquired during winter by *Onstott et al.* [1982] and (*b*) water and thin first-year (ThFY), medium first-year (MFY), and multiyear (MY) sea ice at 1.5, 5.2, 9.6, 13.6, and 16.6 GHz at HH polarization during midsummer when the bulk wetness is 5% by volume (July 5, MIZEX '84).

(about 4%) shows the characteristics of an ideal blackbody, which absorbs all incident radiation, reflecting none, and is a perfect emitter.

Data acquired in conjunction with the above show that backscatter is relatively weak (Figure 9*b*), and data demonstrate further the effective absorption of the incident energy by the thoroughly wet snow layer. Roughness measurements indicate that its surface was smooth at these radar wavelengths (an rms roughness of about 0.3 cm); smooth surfaces produce weak backscatter at angles off vertical.

In review, when the snow scattering volume is reduced to a few centimeters and the snow thickness is at its annual maximum, the wet snow is extremely effective in masking surface ice features at frequencies as low as 5 GHz.

Midsummer

By midsummer the snowpack has experienced considerable melt. Drained snow attains a wetness of about 6% throughout its interior. As is illustrated in the snow wetness diagram in Figure 3*c*, meltwater continues to accumulate on the MY and TFY ice sheets, creating a slush layer several centimeters thick. Draining of water into depressions on TFY and MY ice contributes to the formation of subsurface melt pools as illustrated in Figure 6*c*. The slight increase in liquid water in the snow now limits the penetration of microwaves to distances less than one wavelength. The microwave observables continue to be dominated by the properties of the top layer. Emissivity increases within increasing frequency and remains "blackbodylike" at V polarization (see Figure 7*d*). With the Brewster effect enhancing the V-polarized radiation, surface reflection is the dominant reflection mechanism. Since the internal scattering in the lossy snow is very small, the Fresnel reflectivity provides a good description of the microwave emission at H polarization at frequencies up to at least 35 GHz.

In Figure 8*b*, radar backscatter data are shown for MY, MFY, ThFY, and open water at a 30° incidence angle. Snow wetness of 5% results in microwave penetration depths of about 50 cm at 1.5 GHz, 6 cm at 5.2 GHz, and 2 cm at 9.6 GHz, 13.6 GHz, and 16.6 GHz. Contrast between MY and ThFY ice improves with decreasing frequency (6 dB at 1.5

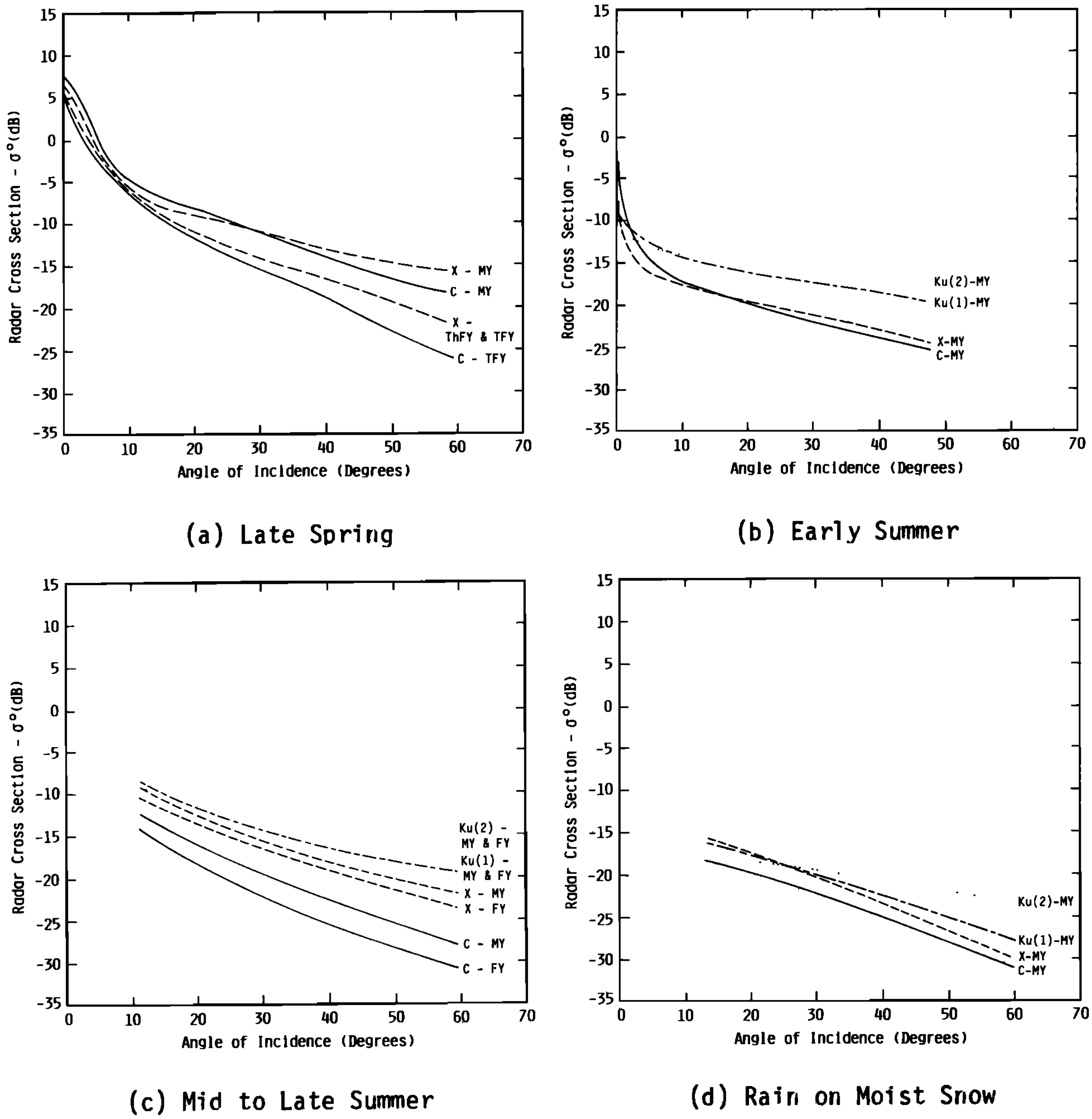

Fig. 9. Radar scattering cross sections acquired during (*a*) late spring of thin first-year (ThFY), medium first-year (MFY), thick first-year (TFY) and multiyear (MY) sea ice at 5.2 (C) and 9.6 (X) GHz at HH polarization when the surface snow is dry and the bulk wetness is 2% by volume (June 20, MIZEX '84), (*b*) early summer of first-year (FY) and multiyear (MY) sea ice at 5.2, 9.6, 13.6 (Ku(1)), and 16.6 (Ku(2)) GHz at HH polarization when the bulk snow wetness is 4% by volume (June 26, MIZEX '84), (*c*) midsummer to late summer of first-year (FY) and multiyear (MY) sea ice at 5.2, 9.6, 13.6, and 16.6 GHz at HH polarization (July 25, MIZEX '83), and (*d*) rainy conditions in summer of first-year (FY) and multiyear (MY) sea ice at 5.2, 9.6, 13.6, and 16.6 GHz at HH polarization (June 25, MIZEX '83).

GHz, 4 dB at 5.2 GHz, and about 2 dB at frequencies from 10 to 17 GHz). Physical property measurements suggest that cross-section differences are attributable to the 2- to 3-cm roughness elements of superimposed ice coupled with the thin snow cover on ThFY and MFY ice (snow thickness is 2–6 cm on ThFY and 2–14 cm on MFY). These data show that uniformly distributed wet snowpack on MY ice with a surface relief greater than 1 m is effective at masking ice features.

Midsummer to Late Summer

Some time after midsummer, open water melt pools become common on thick ice. About 50–60% of the snow has melted (about 1 cm per day). A snow-ice crust is in place on elevated MY ice surfaces, on ThFY ice, and on MY ice. The residual snowpack and snow-ice crust are wet (about 6%). On ThFY and MFY ice the snowpack has eroded into a 2-cm-thick, granular snow-ice layer, and former melt pools consist of collections of candled ice tips which rise about 1 cm above the freeboard of the thin, saturated ice sheet (see Figure 5*d*).

Natural scene intervariability makes it difficult to determine if emission varies with ice type during this period. The data show a keen sensitivity to small physical-property variations in the snow-ice layer, such as density, depth of all the layers, grain size, and wetness. A larger variability in the dielectric

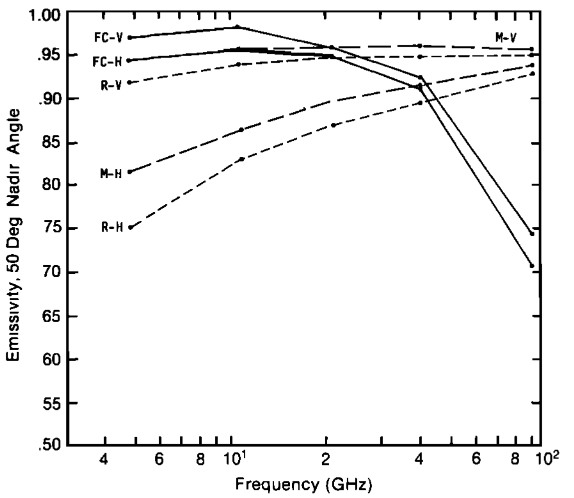

Fig. 10. Emissivity at 50° off nadir in both vertical (V) and horizontal (H) polarization versus frequency representing both multiyear and first-year ice measured during rainy (R) weather with UW/RAD when the snow wetness is about 8% by volume (June 24, MIZEX '84), midsummer with PAMIR when the moist (M) snow wetness is about 5% by volume (July 7–9, MIZEX '83), and midsummer with PAMIR and UW/RAD when the upper layer of the snowpack is a frozen crust (FC) (July 11, MIZEX '83; June 26, MIZEX '84).

constant of FY ice was noted during this period. It is believed that the thinner snow depth observed on FY ice allows sensing of the liquid water which has collected at certain locations on the ice surface. On average it is felt that the emissions of FY and MY ice are still very similar. Emissivities shown in Figure 7*e* are slightly higher than those shown for midsummer.

Backscatter from MY ice is greater than or equal to that from FY ice; a contrast reversal has taken place. Contrast between ice types increases with decreasing frequency, shown in Figure 9*c*. After midsummer, FY ice roughness elements have been eroded by melt to a point where they are small in relation to the radar wavelength; surfaces appear smooth and produce weak backscatter (see Figure 5*d*). Multiyear ice remains topographically more rough and has many tilted surfaces and a complex mixture of ice, snow, and water features which provide a strong surface scatter (see Figure 6*d*).

Very Heavy Melt or Rain

Heavy melt or rain causes a saturation in the upper portion of the snowpack, illustrated in the free water versus depth diagram shown in Figure 4*a*, and reduces the H-polarized emission as shown in Figure 10. In this example the emissivity at 5 GHz for early summer conditions is reduced from 0.86 to 0.75 when rain increased the surface wetness from 4% to 8%. The input of additional free water increases the dielectric constant. The V-polarized emission is less sensitive to this change due to Brewster angle effects. The reflectivity at V polarization is small, and changes in dielectric constant have a correspondingly minor effect. At H polarization a change in dielectric constant translates into a significant change in reflectivity and emission. In addition, as the wavelength increases, the surface now composed of wet snow grains and water looks physically and electrically smoother. This combination works together to reduce emission at this polarization and at low frequencies dramatically. Backscatter intensity was also reduced, reaching its summer low (see Figure 9*d*). Much of this reduction is attributed to the creation of a more specular surface.

Frozen Surface Crust

During periods when long-wave heat loss dominates, such as under cloud free conditions, or when weather systems reduce air temperatures, the upper portion of the snowpack or snow-ice layer freezes, forming a crust. The wetness-depth diagram is provided in Figure 4*b*. An additional circumstance of interest is the mixture of cloud free and cloudy skies. Cloud free skies may produce regions with frozen surfaces; cloud-covered regions a few kilometers away may be under melt because of atmospheric radiation.

Freezing of a snow layer was limited to the upper 5 cm typically. The crust that forms has an important characteristic of snow crystal grain sizes which have enlarged to about 1.5–2 mm in diameter. The increase in size is attributed to the refreezing process. Emissivity at 37 and 94 GHz is reduced significantly because of scattering within this layer. The level of decrease in emission correlates with crust thickness. It is important to note the similarity in emission at 94 GHz between a frozen snow layer with enlarged ice crystals and snow-covered winter MY ice. At the lower frequencies the wavelengths are large compared to the size of the ice crystals in the thin crust, so scattering losses are small and the emission is not reduced. This scattering behavior can be understood by examining Rayleigh scattering of densely packed ice particles [*Matzler*, 1985].

The formation and disappearance of a frozen crust contributes to the large variability seen in the 37-GHz SMMR data during summer (Figure 2). In contrast, note that the 18-GHz signature is less dynamic. This is expected if the upper snow layer is undergoing melt-freeze cycling and not changes in ice concentration. The effect of frozen crust on backscatter is interesting. An increase in backscatter is expected for all ice types at frequencies above 5 GHz due to an enhanced volume scatter. Such an enhancement is not noted in these data. However, the relative contrast between ice types is expected to be preserved and is. The freezing of a thin layer of ice on open melt pools produces a significant increase in backscatter (observed in scatterometer data) for this feature and changes the floe's appearance in the radar imagery.

SUMMARY

Emissions at 5–94 GHz and backscatter at 1–17 GHz were measured for a variety of sea ice scenes present in the summer at the marginal ice zone. Data were obtained with ship-, sled-, and heliocopter-mounted instruments. Meltwater, snow thickness, the freezing of the upper few centimaters of a snow layer, and snowpack and ice surface morphology control the microwave signature of sea ice. During the first half of summer the high absorptivity of a thick, wet snow greatly reduces the variability in sea ice microwave signatures.

Results during the peak of summer melt indicate that physical processes within one penetration depth in snow (less than a wavelength) are adequate to dominate the microwave response and mask surface ice features. This does not mean that all ice sheet information is lost during summer. Snow and meltwater are not distributed uniformly about a floe. The distribution of free water is often related to snow thickness and construction and to ice sheet type and deformation characteristics. These ice-type-related surface nonuniformities are not well understood and are being examined to see if they produce identifiable two-dimensional microwave signature characteristics. The importance of surface features is illustrated by examining the cause of the large variance observed in the SMMR brightness temperature data shortly after midsummer. Our observations show a correlation with a peak in the areal extent of open water within floe boundaries on thick ice; the more open water, the lower the average brightness temperature. Note that prior to this, meltwater collected in subsurface pools did not affect the average scene microwave response. Future rises and falls in brightness temperature may coincide with melt-drain cycling. However, as the end of summer is approached, the contribution to the signature by a melt-induced reduction in ice concentration is expected to be much greater.

The emissions of FY and MY ice during summer were nearly identical. The passive microwave data show an ability to map the spatial distribution of wetness in the upper layers in the snowpack within floe boundaries. The emission at 95 GHz was dramatic in its response to the freezing and melting of the upper few centimeters of the snow layer.

Multiyear and FY ice backscatter underwent multiple contrast reversals. During winter and late spring, MY ice cross sections are larger than those of FY ice due to strong volume scatter from the upper portion of the ice sheet. Wet snowpack, with a maximum seasonal thickness during early summer, causes similar signatures for each of these ice types. By midsummer, ThFY ice backscatter is stronger due to an increased small-scale roughness from a superimposed ice layer which forms at the snow-ice interface and a snow thickness reduced by melt. After midsummer the backscatter contrast again reverses (at the lower frequencies). The ThFY roughness elements are smoothed by melt, and MY ice continues to have a complex surface topography. Based upon the results to date, operation at frequencies of about 5 GHz may be optimal for the summer MIZ.

Results suggest that the ability to discriminate between the various ice types during summer is closely linked to our ability to continuously monitor the distribution of wetness features within floe boundaries. There is synergism in using both active and passive microwave sensors when wetness features are fully developed; the radiometer senses the scene wetness and volume scattering properties, and the radar senses scene wetness, volume scattering properties, and roughness.

Acknowledgments. This work has been made possible by continuing support from the Office of Naval Research under contracts N00014-81-K-0460 and N00014-85-K-0200 and under the National Aeronautics and Space Administration grant NAGW-334.

REFERENCES

Campbell, W. J., R. O. Ramseier, W. F. Weeks, and P. Gloerson, An integrated approach to the remote sensing of floating ice, in *Proceedings Third Canadian Symposium on Remote Sensing*, pp. 36–72, Canadian Aeronautics and Space Institute, Ottawa, Ont., 1975.

Gogineni, S. P., R. G. Onstott, R. K. Moore, Y. S. Kim, and D. B. Bushnell, Mobile microwave spectrometer for backscatter measurements, *Microwaves Radio Frequency*, *23*, 156–166, 1984.

Gray, A. L., R. K. Hawkins, C. E. Livingstone, L. Drapier Arsenault, and W. M. Johnstone, Simultaneous scatterometer and radiometer measurements of sea-ice microwave signatures, *IEEE J. Oceanic Eng.*, *OE-7*(1), 20–32, 1982.

Grenfell, T. C., and A. W. Lohanick, Temporal variations of the microwave signatures of sea ice during the late spring and early summer near Mould Bay NWT, *J. Geophys. Res*, *90*(C3), 5063–5074, 1985.

Hallikanen, M., F. T. Ulaby, and M. Abdelrazik, The dielectric behavior of snow in the 3 to 37 GHz range, in *Proceedings IGARSS'84*, *Spec. Publ. ESA SP-215*, pp. 169–174, European Space Agency, Paris, 1984.

Johannessen, O. M., and D. Horn (Eds.,), MIZEX 84 summer experiment PI preliminary reports, MIZEX Bulletin V, *Spec. Rep. 84-29*, 176 pp., U.S. Army Cold Reg. Res. and Eng. Lab., Hanover, N. H., 1984.

Kim, Y. S., R. G. Onstott, and R. K. Moore, Effect of snow cover on microwave backscatter from sea ice, *IEEE J. Oceanic Eng.*, *OE-9*(5), 383–388, 1984*a*.

Kim, Y. S., R. K. Moore, and R. G. Onstott, Theoretical and experimental study of radar backscatter from sea ice, *Rep. 331-31*, 168 pp., Remote Sensing Lab., Univ. of Kans., Lawrence, 1984*b*.

Livingstone, E. C., R. K. Hawkins, A. L. Gray, K. Okamoto, T. L. Wilkinson, S. Young, L. Drapier Arsenault, and D. Person, Classification of Beaufort Sea ice using active and passive microwave sensors, in *Oceanography From Space*, edied by J. F. R. Gower, pp. 813–826, Plenum, New York, 1981.

Lohanick, A. W., and T. C. Grenfell, Variations in brightness temperature over cold first-year sea ice near Tuktoyaktuk, Northwest Territories, *J. Geophys. Res.*, *91*(C4), 5133–5144, 1986.

Matzler, C., Interaction of microwaves with natural snow cover, Habilitationsschrift, 152 pp., Inst. of Appl. Phys., Univ. of Bern, Bern, Switzerland, 1985.

Matzler, C., R. O. Ramseier, and E. Svendsen Polarization effects in sea-ice signatures, *IEEE J. Oceanic Eng.*, *OE-9*, 333–338, 1984.

MIZEX Group, MIZEX East 83/84: The summer marginal ice zone program in the Fram Strait/Greenland Sea, *Eos Trans. AGU*, *67*, 513–517, 1986.

NORSEX Group, The Norwegian remote sensing experiment in a marginal ice zone, *Science*, *220*(4599), 781–787, 1983.

Onstott, R. G., and S. P. Gogineni, Active microwave measurements of Arctic Sea ice under summer conditions, *J. Geophys. Res.*, *90*(C3), 5035–5044, 1985.

Onstott, R. G., R. K. Moore, S. Gogineni, and C. V. Delker, Four years of low altitude sea ice broadband backscatter measurements, *IEEE J. Oceanic Eng.*, *OE-7*(1), 44–50, 1982.

Ramseier, R. O., and D. J. Lapp (Eds.), Proceedings Final, SURSAT Ice Workshop, 563 pp., SURSAT Project Office Report, Atmos. Environ. Ser., Ottawa, Ont., Canada, 1980.

Tiuri, M., A. Sihvola, E. Nyfors, and M. Hallikainen, The complex dielectric constant of snow at microwave frequencies, *IEEE J. Oceanic Eng.*, *OE-9*(5), 377–382, 1984.

Tucker, W. B., III, A. J. Gow, and W. F. Weeks, Physical properties of summer sea ice in the Fram Strait, *J. Geophys. Res.*, this issue.

T. C. Grenfell, Department of Atmospheric Sciences, University of Washington, Mail Stop AK-40, Seattle, WA 98195.

C. A. Luther, Office of Naval Research, Arctic Sciences, Code 1125AR, 800 N. Quincy Street, Washington, DC 22217.

C. Matzler, Institute of Applied Physics, University of Bern, Sidlerstrasse 5, CH-3012, Bern Switzerland.

R. G. Onstott, Environmental Research Institute of Michigan, Advance Concepts Division, Radar Science Laboratory, P. O. Box 8618, Ann Arbor, MI 48107.

E. A. Svendsen, Geophysical Institute and Nansen Ocean and Remote Sensing Center, University of Bergen, N-5037 Solheimsvik, Norway.

(Received November 20, 1986;
accepted February 4, 1987.)